Accepted Manuscript

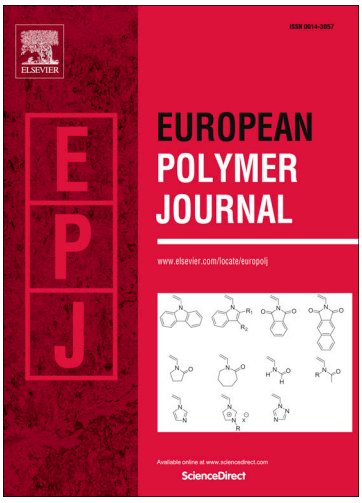

Correlation between mechanical dissipation and improved X-band electromagnetic shielding capabilities of amine functionalized graphene/thermoplastic polyurethane composites

Azam Nasr Esfahani, AliAsghar Katbab, Aidin Taeb, Leonardo Simon, Michael A. Pope

PII: S0014-3057(17)31086-8
DOI: http://dx.doi.org/10.1016/j.eurpolymj.2017.08.038
Reference: EPJ 8031

To appear in: *European Polymer Journal*

Received Date: 21 June 2017
Revised Date: 17 August 2017
Accepted Date: 22 August 2017

Please cite this article as: Nasr Esfahani, A., Katbab, A., Taeb, A., Simon, L., Pope, M.A., Correlation between mechanical dissipation and improved X-band electromagnetic shielding capabilities of amine functionalized graphene/thermoplastic polyurethane composites, *European Polymer Journal* (2017), doi: http://dx.doi.org/10.1016/j.eurpolymj.2017.08.038

Correlation between mechanical dissipation and improved X-band electromagnetic shielding capabilities of amine functionalized graphene/thermoplastic polyurethane composites

Azam Nasr Esfahani[a,c] , AliAsghar Katbab[a*], Aidin Taeb[b], Leonardo Simon[c], Michael A. Pope[c*]

Abstract

Graphene-based polymer nanocomposites have demonstrated significant promise to create commercially viable electromagnetic interference (EMI) shielding to protect the next-generation of electronic materials from radiative pollution. In the present study, we carry out a systematic analysis of the dynamic mechanical, dielectric, electrical and X-band shielding properties of thermoplastic polyurethane (TPU) elastomer filled with amine functionalized graphene obtained by the rapid thermal expansion of graphite oxide. By preparation of nanocomposites based on modified and unmodified graphene using solution mixing and hot compression moulding, we demonstrate that the modification with 2-aminoethyl methacrylate enhances the EMI shielding from 14 to 25 dB. We also show by fracture analysis, cross-sectional transmission electron microscopy and dynamic mechanical analysis that the modification significantly strengthens the interfacial interactions between TPU and the functionalized graphene at the same filler loading. We find that the dominant shielding mechanism is through absorption and discuss the correlation between the viscoelastic mechanical loss tangent and the more effective dissipation of absorbed EM radiation which might account for the discrepancy between the theoretically predicted and experimentally observed EMI SE.

Keywords: thermoplastic polyurethane, graphene, electromagnetic interference shielding, viscoelastic properties, interfacial interaction

Introduction

Electromagnetic interference (EMI) consists of undesirable and uncontrolled radiated signals emitted by electronic instruments [1,2] which can interfere with the normal operation of other electronic devices [3–5]. Therefore, an appropriate EMI shield is necessary to protect workspaces and the environment from electromagnetic waves, specifically in the X-band frequency (8.2– 12.4 GHz) [4] used by many critical applications such as weather radar, air traffic control, satellite communications, and television broadcasting [6]. This has led to significant efforts to fabricate improved EMI shielding materials [7]. Metals and metallic composites have high shielding efficiency due to their high electrical conductivity but are physically rigid, relatively heavy and susceptible to corrosion [8]. On the other hand, conductive polymer composites (CPCs) overcome most of these challenges as they are light weight, relatively low cost, and can be easily solution cast or melt processed at low temperatures [9]. The shielding effectiveness (SE) of CPCs is known to be governed by the polymer and filler properties, filler dispersion state, and polymer-filler interfacial interactions. Therefore, in recent years, many studies have investigated various combinations of polymers and fillers to create CPCs with improved electrical conductivity and at low filler content (i.e., fillers with low percolation threshold). Many polymers, such as epoxies [6,10,11], poly (methyl methacrylate) (PMMA) [12], polyethylene (PE) [13], poly (ethylene vinyl acetate) [14], polypropylene (PP) [4], polystyrene (PS) [15] and polyurethane [16–18] have been employed as polymer matrices. Of these matrices, thermoplastic polyurethane (TPU) elastomer is gaining increasing attention due to its widespread commercial use in consumer electronics resulting from its desirable properties such as scratch resistance and ease of processing.

Also, many studies have been devoted to different types of conductive carbonaceous fillers [19] such as carbon nanotubes (CNT) [6,20], carbon blacks (CB) [21,22], graphene-based materials [11], and carbon fibers [23]. Among these various conductive fillers, graphene-based materials are promising due to their high aspect ratio, excellent mechanical, electrical and thermal properties [24–27].

Recent work has focused on improving the dispersion state of the filler in efforts to improve the electrical conductivity and thus the SE [5,19,20,24,28]. Several of these works have studied the effect of modifying the interface between the polymer and filler to improve filler-matrix compatibility

[a.] *Department of Polymer Engineering, Amirkabir University of Technology, P.O. Box 15875-4413, Tehran, Iran.(a* katbab@aut.ac.ir)*
[b.] *Department of Electrical and Computer Engineering, University of Waterloo, Waterloo, ON N2L 3G1, Canada.*
[c.] *Department of Chemical Engineering, University of Waterloo, Waterloo, ON N2L 3G1, Canada.(c* michael.pope@uwaterloo.ca)*

[15,29,30]. For example, Hsiao and co-workers [30] studied the effect of non-covalent graphene modification on the EMI SE of water-born polyurethane (WPU)/ reduced graphene oxide (rGO) composites and attributed the improved EMI shielding effectiveness to an improved dispersion state of the filler which affected an increase in electrical conductivity. However, they found that the weak interaction between surfactant and rGO leads to unstable filler dispersion. Thereafter, they used a covalent modification of rGO to facilitate interactions with the polymer matrix [24]. They concluded that the electrical conductivity and consequently EMI shielding of WPU/rGO composites can be affected by the compatibility between the rGO and WPU. Chhetri and co-workers [31] used sulfanilic acid azo-chromotrop (SAC) to functionalize the surface of graphene in order to improve EMI SE of graphene/epoxy nanocomposite. Their results revealed that the $–SO_3H$ groups of SAC interacted with –OH groups in epoxy segments leading to uniform dispersion and higher interfacial interactions between the polymer matrix and graphene. They attributed the improved EMI shielding properties of the composites to the improved filler dispersion which resulted in a high electrical conductivity at low filler loading. Others have employed hybrid systems of conductive fillers in order to improve the electrical conductivity and consequently EMI SE of the composites by means of the synergistic effect of two or more different fillers [32–34]. Chen and co-workers [35,36] showed that the rGO-carbon fiber (CF) improves the EMI SE of unsaturated polyester based composites more than CF due to the significant improve in dispersion state. Verma *et al.* [37] studied the EMI SE of a nanocomposite comprised of TPU and a graphene-carbon nanotubes hybrid (GCNT) which exhibited excellent EMI shielding (30-47 dB) for a composite containing 10 wt% of GCNT. Since the tan δ_ε (the ratio of imaginary to real part of permittivity) represents the ability of the materials to absorb EM wave energy, they investigated the dielectric permittivity of the nanocomposites as a function of frequency. Their results revealed that the increasing GCNT loading leads to an increase in tan δ_ε and EMI SE.

Generally, good flexibility, small effective thickness, and low filler content (to reduce costs) are important features for commercial adoption of EMI shielding materials. Since high conductive filler loading is required to reach CPCs with high electrical conductivity, fabricating CPCs with desired shielding SE, small thickness and good flexibility still remains a challenge [38]. The EMI SE of select CPCs based on graphene as a conductive filler are presented in Table 1. In most cases, commercially relevant shielding effectiveness (> 20 dB) is achieved for either relatively thick films (2-6 mm) or high filler loading (10-20 wt%). While some thin film results have demonstrated impressive results, these require layered structures of a mechanically fragile, high loading graphene layer with another polymer coating. For example, Shen *et al.* [39] prepared a sandwich structure consisting of a high conductivity TPU/graphene composite and a polyester non-woven fabric as reinforcing interlayer. The SE of their film with 20 wt% graphene and total coating thickness of ~50 µm exhibited EMI SE of ~15 – 26 dB. Therefore, there remains a need to investigate new combinations of materials, mechanisms and strategies to create thinner films at lower loadings to reduce costs and improve flexibility in manufacturing. Beside material properties, a deeper understanding of the EMI shielding mechanisms is required to optimize the EMI shielding effect of polymer nanocomposites with minimum filler loading and cost.

In particular, the EMI SE, is dependent on the amount of radiation that is either reflected, absorbed or undergoes multiple reflections. A wave is reflected when there is an impedance mismatch between the two materials [40] and is the result of EM wave interactions with the mobile charge carriers (electrons or holes) in the filler. Therefore, electrically conducting materials are the best choice for this mechanism, although a high conductivity is not required [41]. Absorption results when an electrical dipole moment within the material interacts with the EM wave travelling through the shield leading to energy dissipation [42–44]. Multiple reflection losses can typically be ignored when the contribution from absorption with respect to the total SE is high (> 10 dB) [19,45]. This is because most of the re-reflected waves are absorbed within the shield. For CPCs, absorption is typically dominant [19,46–48], and thus the EMI SE is governed by the reflection and absorption mechanisms only. Shielding by absorption is mainly the results of time-dependent dipole polarizations which leads to the attenuation of the incident EM wave energy [8]. When the material is subjected to an electromagnetic field, several dielectric polarization processes occur depending on the wave frequency [49]. These include electronic, atomic, orientational and interfacial processes known as Maxwell-Wagner-Sillars (MWS) polarizations [50,51]. Orientation and interfacial dipole polarizations have a larger dependence on time scale compared with electronic and atomic polarizations. Hence, orientation polarization decreases with increasing frequency. Also, interfacial polarization is also a larger effect at lower frequencies [50]. Orientation polarization is mainly governed by the ease of polymer molecular motion and consequently the degree of polymer-filler interactions which act to dampen the polarization [52].

Since CPCs exhibit viscoelastic features, when they are subjected to an oscillating mechanical or electrical field, they exhibit damping behaviour which can dissipate the field energy. The extent of energy damping by a polymeric material depends on the numbers and ease of viscous molecular motions. Therefore, the chemistry of both filler and polymer and hence the types of interfacial interactions likely play an important role in the extent of energy damping [53]. Based on the dielectric and viscoelastic behaviour of CPCs, it seems plausible that the dynamics of the polymer-filler interactions may play an important role in dissipating EM wave energy.

Table 1. EMI shielding effectiveness in composites based on graphene and related materials.

Composite type	Filler amount	Thickness	EMI SE (dB)	Frequency	Ref.
TPU/rGO	20 wt.%	50 µm	~20	X band	[39]
TPU/EG	20 wt.%	4mm	16-22	X band	[54]
TPU/G/CNT	10 wt.%	3mm	30-47	Ku band	[37]
Epoxy/rGO	15 wt.%	2.0 mm	21	X band	[11]
SiO_2/rGO	20 wt.%	1.5 mm	36-37	X band	[55]
UHMWPE/TRGO	0.660 vol.%	2.5 mm	28.3–32.4	X band	[56]
PS/rGO	3.47 vol.%	2.5 mm	45.1	X band	[57]
PS/FGN(foam)	30 wt.%	2.5 mm	29	X band	[58]
PEI/rGO	10 wt.%	2.3 mm	20	X band	[59]
PMMA/rGO	8 wt.%	3.4 mm	30	X band	[60]
Phenolic/rGO	70 wt.%	0.2-0.4 mm	43.42	X band	[61]
PS/TRGO(foam)	10 wt.%	2.8 mm	18	X band	[62]
PS/rGO/MWCNT	1.5 wt% rGO+2 wt.% MWCNT	5.6 mm	20.2	X band	[63]
PMMA(foam)/rGO	1.8 vol.%	2.4 mm	13-19	X band	[64]

To the best of our knowledge, no works have been reported concerning the relationship between dynamic mechanical characteristics and electromagnetic wave shielding behaviour of polymer composites comprising conductive nanofillers. In the present work, we have systematically studied the correlation between mechanical damping and the EMI SE of TPU/thermally reduced graphene oxide (TRGO) nanocomposites. For this purpose, polyester-based TPU has been employed as the polymer matrix because of its excellent mechanical properties [17,65]. Also, the presence of polar groups in TPU chains is hypothesized to lead to an increase in orientation polarization [66]. On the other hand, TRGO produced by the rapid thermal expansion of graphite oxide contains a significant number of defects and functional groups which are known to improve EM wave absorption [67]. To examine the influence and extent of TPU/TRGO interactions and the chemistry of the TRGO surface upon modification with 2-aminoethyl methacrylate (AEMA) as a long and polar chain, both mechanical and dielectric damping characteristics were studied. Modification of TRGO, leads to a significantly enhanced elastic modulus but also leads to a more significant change in the loss modulus. The SE via absorption loss increased from 12.2 dB to 21.1 dB (at 9.5 GHz) for the composite comprising 5 vol. % of unmodified and modified TRGO, respectively, for samples only 1 mm thick. All nanocomposites at various filler loadings exhibited similar characteristics. Since there was only a small change in composite electrical conductivity (AC and DC) between modificed and unmodified samples, and the SE via reflection was not significantly affected, we attribute the enhanced shielding effectiveness to the improved mechanical loss tangent. More effective stress transfer due to stronger polymer–TRGO interactions together with improved dispersion of TRGO particles is thought to enhance viscous energy dissipation upon the absorption of electromagnetic radiation.

Experimental section

Materials

Thermoplastic polyurethane Kuramiron™ 8165 (TPU) with a density of 1.14 g/cm^3 (20 °C), melt viscosity of 1.1 kPa.s, and 65 Shore A hardness was kindly provided by Kuraray (USA) and was used as received. Natural graphite powder with a purity > 99.9% was supplied by Alfa Aesar (USA). Sulfuric acid (H_2SO_4), phosphoric acid (H_3PO_4), hydrogen peroxide (H_2O_2, 30%), potassium permanganate ($KMnO_4$), 2-aminoethyl methacrylate hydrochloride (AEMA), and potassium peroxodisulfate (KPS) were purchased from Sigma-Aldrich Co. (USA). N,N-dimethyl formamide (DMF) (Sigma-Aldrich, 99% purity) was used to dissolve TPU and disperse the TRGO fillers.

Preparation of TRGO and modified TRGO (mTRGO)

Tour's improved Hummers method [68] was employed to synthesize graphene oxide (GO). Briefly, 40 ml of H_3PO_4 and 360 ml of H_2SO_4 were mixed in a three-necked flask which was placed in the ice bath. Then, 18 g of $KMnO_4$ was slowly poured into the solution while the temperature was kept below 25°C to prevent the generation of potentially explosive potassium manganese heptoxide. Subsequently, 3 g of graphite powder was gradually added to the mixture under continuous stirring. The solution was further stirred at 45 °C for 16 hrs to obtain a highly viscous fluid. Hydrogen peroxide (30%) was gradually added to the cooled mixture until the solution color changed from purple to bright yellow. To obtain a pure GO solution, the resulting mixture was centrifuged and washed twice with water, once with diluted HCl (10%) and four times with ethanol to remove the residual acids and salts. The washed GO was dispersed into de-ionized water and dried using a Buchi Mini Spray Dryer B-290 to obtain a powder. Thermal reduction of the GO powder was carried out by placing 60 mg of GO into a long quartz tube which was rapidly inserted into a Lindberg Minimite tube furnace preheated to 1100 °C and held for 2 minutes to obtain the TRGO.

To modify the TRGO, 1.0 g of TRGO was added into 300 ml de-ionized (DI) water and the solution was magnetically stirred for 2 hrs followed by 1 hr sonication at room temperature to ensure uniform dispersion of TRGO particles in the solution. Then, 1 g AEMA and 15 mg KPS were added to the TRGO dispersion. This mixture was refluxed at 90°C under N_2 purging for 10 hrs. Under these conditions the AEMA can polymerize via free-radical polymerization and is expected to graft onto the surface of TRGO as shown schematically in Fig. 1 [24]. The resulting product was washed repeatedly by centrifugation with DI water to remove unreacted AEMA. The final product was freeze dried and subjected to various analyses.

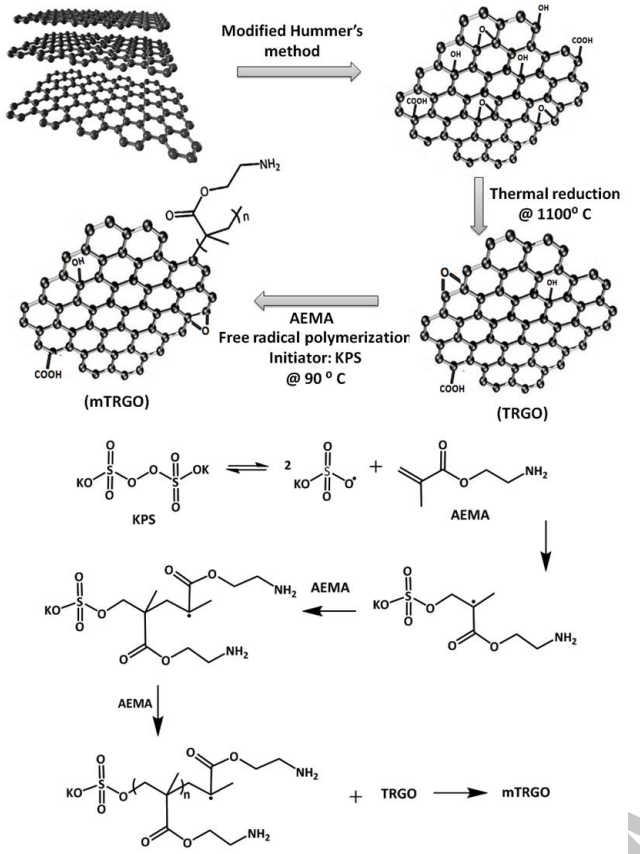

Fig. 1. Scheme of mTRGO preparation procedure. It is known that TRGO contains abundant reconstructed vacancy and topological defects that are not shown for simplicity [24].

Preparation of TPU/TRGO composites

Nanocomposites with various loadings of TRGO were fabricated by solution mixing. Ten grams of TPU was dissolved in 300 ml of DMF heated to 50 °C and then subjected to vigorous stirring for 1 hr. Different amounts of TRGO (modified or unmodified), depending on the required amount of TRGO in the final nanocomposite, were dispersed in DMF and treated under bath ultrasonication for 2 hrs. Subsequently, the sonicated mixture was fed into the TPU/DMF solution and was agitated at 25 °C for 1 hr to obtain a homogeneous suspension solution. Then, the TPU/TRGO mixture was added dropwise into DI water and then repeatedly washed with DI water. The washed mixture was left over night to dry. Finally, the samples were subjected to additional drying at 70 °C in a vacuum oven for 4 hrs to remove all traces of solvents prior to hot compression moulding at 200 °C to form sheets with different thickness for further characterization.

Characterization methods

X-ray photoelectron spectroscopy (XPS) was carried out with a Thermo-VG Scientific ESCALAB 250 (USA) microprobe which uses a monochromic Al K_α source to examine the composition of GO, TRGO and mTRGO. Energy-dispersive X-ray spectroscopy (EDS) VEGA (TESCAN, Czech Republic) was also applied for elemental analysis and mapping to verify the distribution of the amine-based coating. Powder X-ray diffraction (XRD) was conducted on TRGO, mTRGO, and the corresponding nanocomposites using a model D8 Bruker (USA) X-ray diffractometer operating at 40 kV and 40 mA with CuK_α radiation (λ = 0.154 nm). The TRGO and mTRGO samples were examined in the form of fine powder, while TPU, TPU/TRGO and TPU/mTRGO composite specimens were analysed in the form of thin hot compression moulded films. The analysis was performed within a diffraction angle range of $2\theta = 3 - 30°$ at a scan rate of 1°/min. Thermal analysis was carried out by thermal gravimetric analysis (TGA) using a Q500 TA Instruments (USA) system. The test was carried out within a temperature range of 30 °C to 600 °C with a heating rate of 10 °C/min under N_2 atmosphere.

The morphology of the prepared nanocomposites was examined by scanning electron microscopy (SEM, AIS2100 Seron technology, Korea). For this purpose, prepared samples were cryo-fractured, and surfaces were sputtered with gold to prevent surface charge accumulation. Transmission electron microscopy (TEM, Philips CM10, The Netherlands) operated at 60 kV was used to examine cross-sections of the composites. Samples for TEM were prepared by first hot pressing composites into films and embedding these separately into epoxy resin (SPI-PON 812), which was cured at 70 °C for 12 h. The cured samples were then subjected to sectioning (70-100 nm thickness) at 80°C using a cryo-ultramicrotome Leica EM FC6 (Austria) equipped with a diamond knife. Dynamic mechanical characteristics of the prepared nanocomposites were studied by dynamic mechanical thermal analysis (DMTA, TA, USA). The hot compression moulded samples with dimensions of 15 mm × 10 mm × 0.4 mm were examined in tension mode at room temperature within the frequency range of 0.1-300 Hz, and within the linear stress-strain regime at the strain amplitude of 0.03.

A four probe electrical conductivity-measuring instrument (model 6514, USA) with 200 mA, 5 kV, was used for measuring the DC electrical conductivity.

Impedance measurements were carried out using an Autolab Frequency Response Analyser System (PGSTAT302N AUTOLAB, The Netherlands) by connecting the sample to two silver electrodes. Dielectric permittivities of the samples with dimensions of 0.4 by 0.9 inches were also measured at the X-band frequency using a vector network analyzer (PNA, Agilent E8364B) and WR90 waveguide.

The EMI shielding effectiveness of nanocomposites was measured using a network analyzer (Agilent N5245A, USA) connected with WR-90 rectangular waveguide as demonstrated in Fig. 2. For this purpose, the required specimens with the dimension of 22.86 mm × 10.16 mm (0.9 in × 0.4 in) × 1 mm were prepared via the hot compression moulding process. The S-parameters of each nanocomposite were evaluated over the X-band frequency.

The EMI SE was estimated from the incident power (P_i) and transmitted power (P_t) using equation 1 [9]:

$$EMI\ SE = -10 \log \frac{P_t}{P_i}, \quad (1)$$

The EMI SE is calculated from the measured S-parameters by equation 2:

$$EMI\ SE = 10\log\frac{1}{|S_{21}|^2} = 10\log\frac{1}{|S_{12}|^2} \quad (2)$$

where S_{ij} denotes the transmitted power from port i to j. Moreover, absorption loss (SE_A), reflection loss (SE_R), absorbed power (A), reflected power (R) and transmitted power (T) were calculated using the S-parameter by employing equations 3 to 8.

$$SE_{tot} = SE_R + SE_A \quad (3)$$

$$SE_R = 10log_{10}\left(\frac{1}{1-|S_{11}|^2}\right) \quad (4)$$

$$SE_A = 10log_{10}\left(\frac{1-|S_{11}|^2}{|S_{21}|^2}\right) \quad (5)$$

$$R = |S_{11}|^2 = |S_{22}|^2 \quad (6)$$

$$T = |S_{12}|^2 = |S_{21}|^2 \quad (7)$$

$$A + R + T = 1 \quad (8)$$

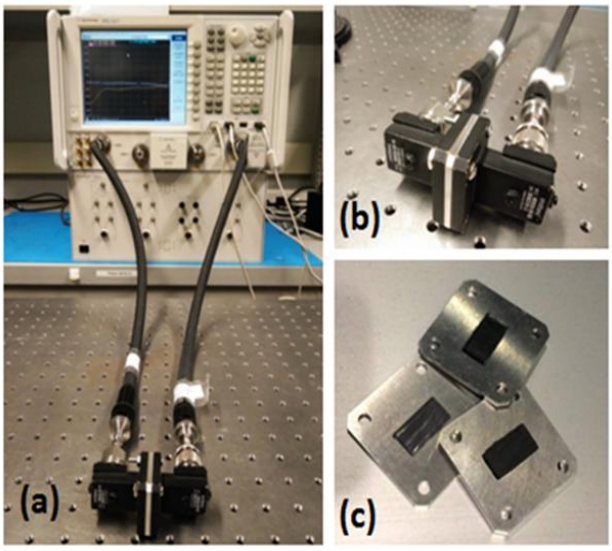

Fig. 2. Schematic of the network analyser used for measuring the S-parameters: (a) network analyzer, (b) waveguides holding the sample, (c) aluminum sample holder.

Results and discussion

In the following sections we first verify the chemical nature of both the TRGO and mTRGO produced and then assess their dispersion state within the polymer matrix. This is followed by a systematic analysis of the mechanical and electrical properties.

Chemical and thermal properties

As shown in Fig. 3(a,b), XPS was conducted on compacted powders of TRGO and mTRGO to determine the detailed chemical composition. There exists five C1s peaks corresponding to the C-C, C-O, C-O-C, C=O, and O-C=O (Fig. 3(a). However, in the spectrum of mTRGO (Fig. 3(b)), one additional C1s peak has appeared at a binding energy of

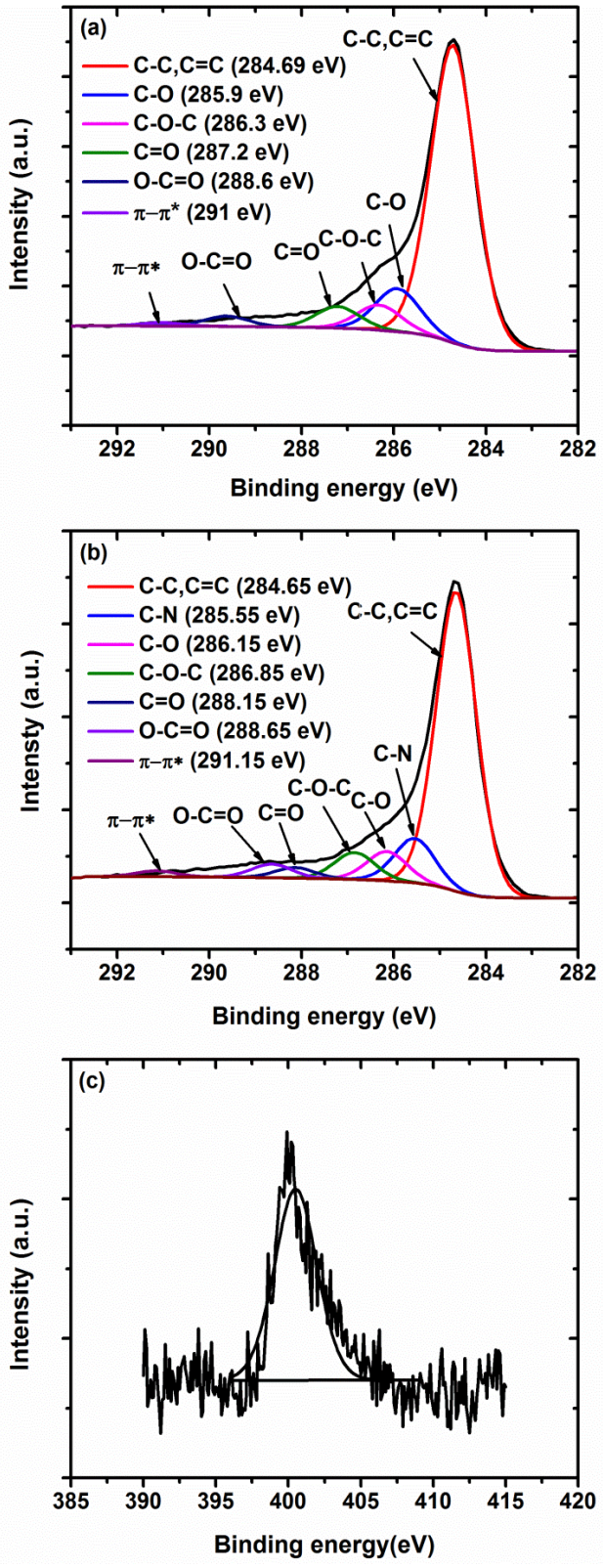

Fig. 3. High resolution XPS spectra: (a) C 1s spectra of TRGO; (b) C1s spectra of mTRGO; (c) N1s spectra of mTRGO.

286.08 eV which corresponds to the C1s of the C-N bond. This suggests the presence of AEMA on the TRGO and confirms that our grafting reaction was successful. This is also evidenced by the N1s appearing in the spectrum of mTRGO as shown in

Fig.3(c). The fraction of nitrogen in the mTRGO sample (10.3 at%) is higher than that reported by Hsiao *et al.* who used a similar procedure to modify TRGO. This might be explained by the extended reaction time used in this work (10 h vs. 8 h).

The presence and distribution of AEMA on the TRGO surface was also confirmed by EDS mapping as shown in Fig. 4a. The TRGO powder was found to be composed of only carbon and oxygen (Fig.4 b,c). For the mTRGO (Fig. 4 d-g), a significant amount of nitrogen was detected throughout the sample which confirm the presence of polymerized AEMA. Furthermore, element mapping shown in Fig. 4 (e-g) confirms a homogeneous distribution of AEMA on the mTRGO surface [69]. While both XPS and EDS indicate a significant coating on the TRGO, it is difficult to prove whether or not this is covalently bound to the graphene or whether some material physisorbed since there was no unique chemical bond identified between graphene and AEMA. However, as discussed later, the significantly strengthened interactions apparent in the thermal and mechanical data suggest that covalent grafting does occur.

Fig. 5(a) illustrates the XRD patterns of TRGO and mTRGO as well as the corresponding TPU nanocomposites. Neither TRGO nor mTRGO exhibit any diffraction peak over the range in 2 θ investigated (3-30°), suggesting that there is no graphite d_{0002} peak expected at $2\theta = 26.8°$ indicating the absence of restacking/aggregation [69–72]. It means that upon oxidation and the rapid thermal expansion of graphite oxide, the resulting TRGO and mTRGO powders show no observable peak near $2\theta \sim 27°$ which indicates that the exfoliation procedure was effective and that the sheets are only weakly aggregated in the powder form [73]. Moreover, no graphite diffraction peak has appeared in the XRD spectrum of corresponding nanocomposites, suggesting no ordered structure for graphene nanosheets, and their well randomly dispersion throughout the TPU matrix [70,74,75]. The neat TPU matrix shows a broad peak at a diffraction angle of $2\theta = 17–23°$ which corresponds to the inter-chain spacing of 0.445 nm within the TPU [76]. This crystallinity is associated with the hard segments in the structure of TPU which are more ordered than the soft segments. As can be observed in Fig. 5(a) (XRD pattern d and e), this peak is also present in the XRD pattern of TPU/TRGO and TPU/mTRGO and indicates that the presence of both fillers does not significantly affect the self-assembly of isocyanate segments during solvent evaporation.

To further investigate the role of enhanced interactions between graphene and TPU segments, thermal gravimetric analysis was conducted on both groups of composites based on TRGO and mTRGO and the obtained thermograms are illustrated in Fig. 5(b). The initial degradation temperature (T_i) is specified as the temperature at 5% weight loss [75]. Comparing the thermograms of the neat TPU sample with those of the composites comprising 2.5 vol. % of unmodified and modified TRGO shows that T_i for the TPU matrix (284.4 °C) is shifted to a higher temperature after modification, 301.8 °C vs. 313.1 °C, respectively. The higher T_i of the nanocomposite of the modified TRGO is attributed to the higher degree of dispersion of mTRGO and also to the enhanced interfacial interaction between TRGO and TPU segments which result in the retardation of thermal motion by the TPU segments confined within the physical networks formed by the TRGO particles [77].

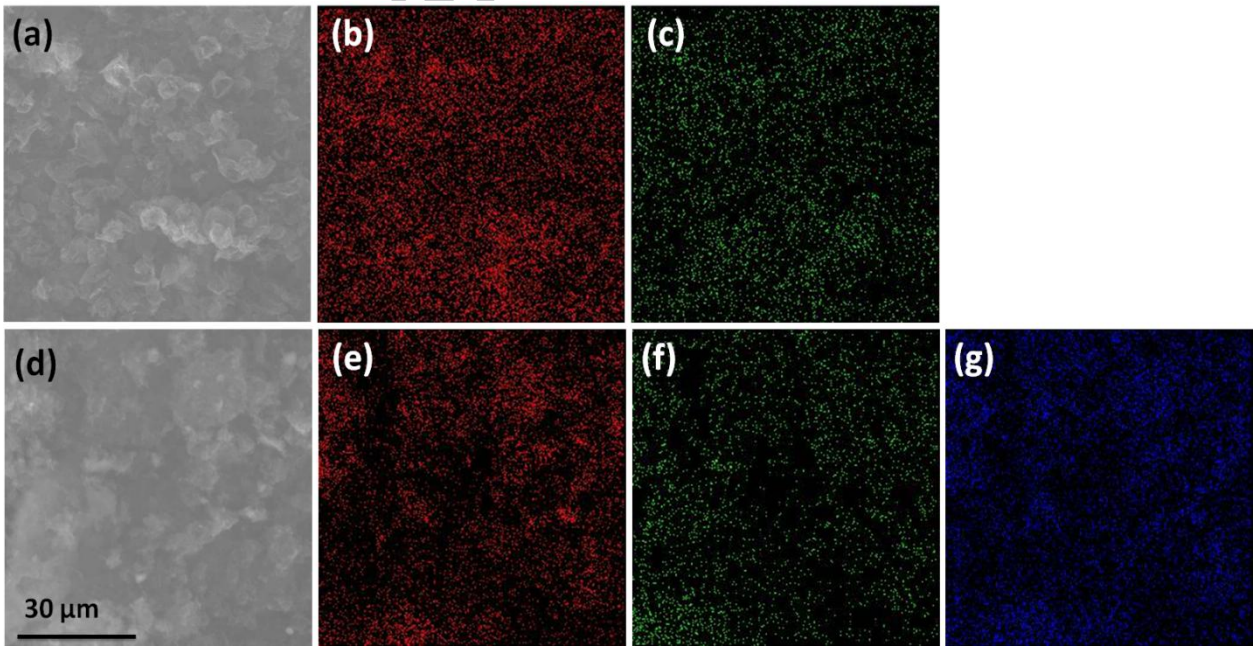

Fig. 4 (a) SEM image of TRGO powder, (b,c) EDS elemental mapping of TRGO for C and O ,respectively, (d) SEM image of mTRGO powder, (e,f,g) EDS elemental mapping of mTRGO for C, O and N, respectively.

Filler dispersion state and fracture analysis

The effectiveness of surface functionalization of TRGO in enhancing the interfacial adhesion with TPU matrix was also evaluated by performing SEM analysis on the cryo-fractured surface of composites prepared with 2.5 vol. % filler loading. The surface of neat TPU exhibits a smooth surface (Fig. 6 a), whereas both composites show a patchy and rough surface due to the presence of TRGO within the TPU. However, the TPU/mTRGO composite shows fractured surfaces which appear rougher (Fig. 6(c)) than fractured surfaces of TPU/TRGO (Fig. 6(b)). This observation suggests stronger interactions between the surface of mTRGO and TPU segments as a result of the surface functionalization [24,78–80].

Improved dispersion and interfacial bonding in the TPU/mTRGO nanocomposite compared to the non-functionalized sample are also evidenced in TEM images presented in Fig. 7(c,d). The mTRGO appears to be more uniformly dispersed throughout the matrix which better facilitates the formation of interconnected conductive networks and leads to an increase in electrical conductivity as will be discussed later.

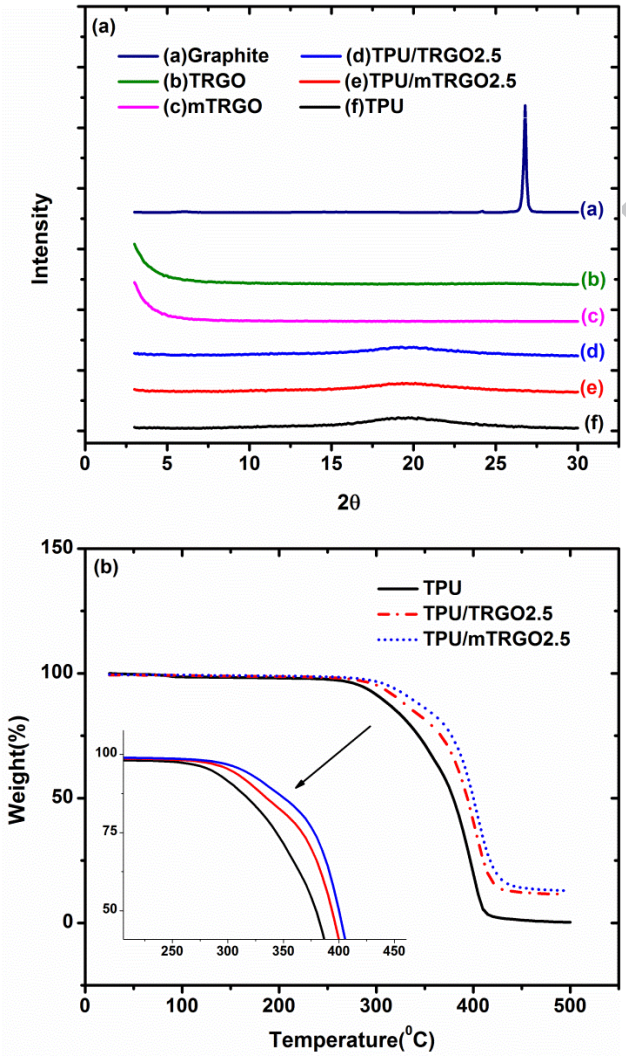

Fig.5. (a) Comparison between XRD pattern of pristine graphite, TRGO, mTRGO, TPU/TRGO, TPU/mTRGO and neat TPU, and (b) TGA thermograms for neat TPU, TPU/TRGO2.5, and TPU/mTRGO2.5 nanocomposites.

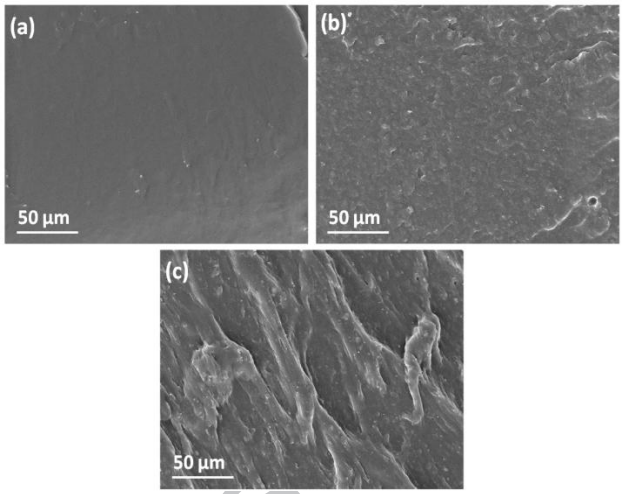

Fig.6. SEM micrographs of cryo-fractures surfaces of (a) neat TPU, (b) TPU/2.5 vol.% TRGO, and (c) TPU/2.5 vol.% mTRGO (e, f).

Dynamic mechanical properties

Dynamic mechanical thermal analysis (DMTA) was used to probe the influence of TRGO dispersion state and polymer/filler interactions on the mechanical properties and molecular structure of the prepared composites. Fig. 8 illustrates the storage and loss modulus (E′ and E″) of unfilled TPU, TPU/TRGO, and TPU/mTRGO nanocomposites as a function of frequency and filler loading. In the low frequency region, E′ for all nanocomposites is higher than the unfilled TPU. This implies that the molecular motions of TPU chains are restricted by the TRGO particles or aggregates. However, the mTRGO shows consistently higher modulus at each loading which is a result of the stronger molecular interactions between the TPU segments and functional groups grafted on the surface of mTRGO. However, the enhanced modulus may also be explained by a higher number density of filler particles within the composite as a result of the somewhat improved dispersion state of mTRGO implied by the TEM results discussed above. These results are also consistent with higher thermal stability of the TPU/mTRGO nanocomposites observed by TGA [81]. All results show the typical and expected monotonic increase of storage modulus with frequency [82]. It is observed that the loss tangent (tan δ) of the nanocomposites generated by mTRGO is much higher (0.10 vs. 0.05 at 1 Hz for 5 vol. % of filler) than TPU/TRGO composite samples. This can be ascribed to the stronger interactions between the surface of mTRGO and TPU segments which leads to retardation of viscous motion and consequently higher viscous energy dissipation of the applied stress field. These results suggest improved damping characteristics of TPU/mTRGO nanocomposites compared to neat TPU and TPU/TRGO counterparts when subjected to an oscillating stress field.

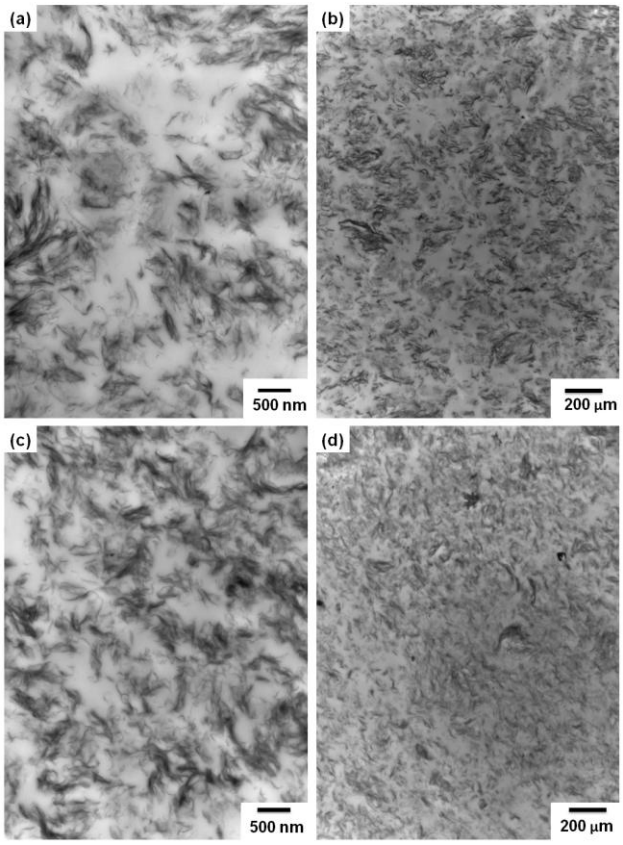

Fig. 7. TEM micrograph of TPU nanocomposites containing 2.5 vol. % of TRGO (a,b) and mTRGO (c,d).

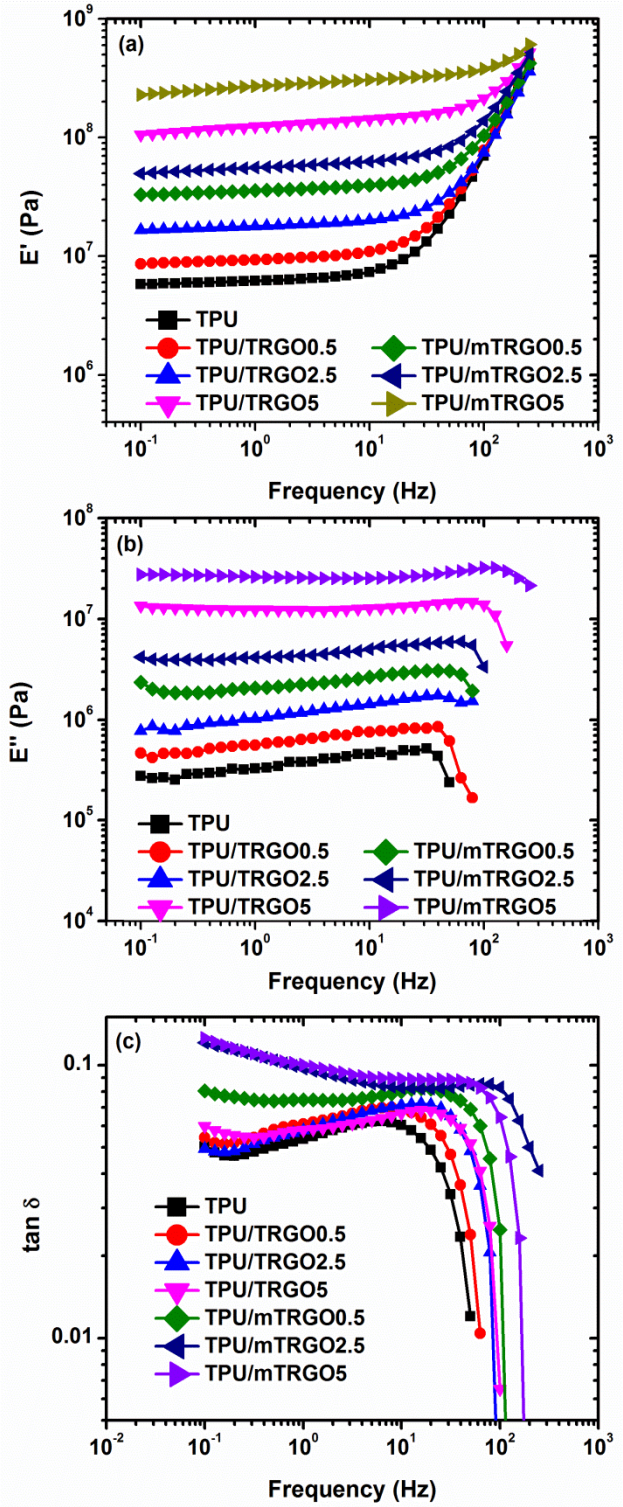

Fig. 8. (a) Storage modulus (E'), (b) loss modulus (E''), and (c) loss tangent (tan (δ)) vs. frequency for the TPU-based nanocomposites.

Electrical conductivity

Fig. 9(a) depicts the DC conductivity of the TPU/graphene composites as a function of filler volume percent. Both groups of composites exhibit a non-linear and sharp increase in conductivity with filler concentration which indicates a transition from an isolated to an interconnected physical network of TRGO dispersed throughout the TPU matrix. The transition from insulating to conductive behaviour for both groups of nanocomposites occurs at 0.5 vol. %. Kim *et al.* [71] report that among the composites based on TRGO, electrical properties of in situ polymerized and solvent-blended samples is better than melt-blended ones. A similar percolation threshold between 0.3 and 0.5 vol. % TRGO is commonly reported in solvent blended samples or those produced by in situ polymerization.

The composites based on mTRGO show higher conductivity at comparable filler concentration with the largest difference (7 vs 0.46 S/m) at a filler loading of 5 vol. %. These are indicative of the improved dispersion state of mTRGO which improves the interconnectivity between the mTRGO particles and also enhances the number of interactions with the host TPU [83].

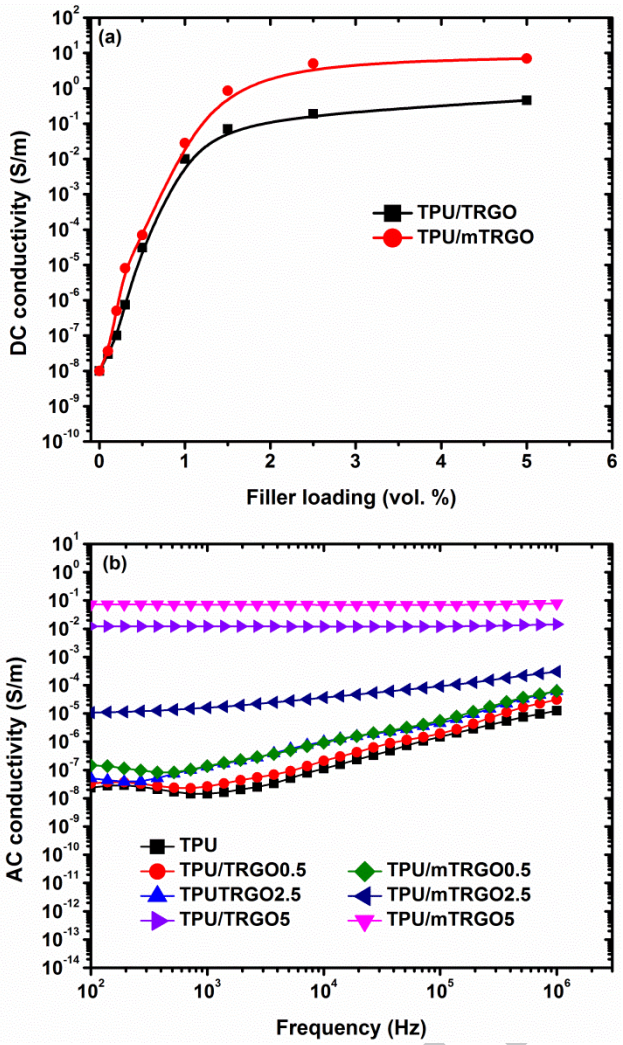

Fig. 9. (a) DC electrical conductivity and (b) AC electrical conductivity of TPU/TRGO and TPU/mTRGO nanocomposites as a function of filler loading.

AC electrical conductivity and its variation with frequency for the reference TPU matrix, TPU/TRGO, and TPU/mTRGO nanocomposites with different TRGO levels are illustrated in Fig. 9 (b). Below the percolation threshold, AC conductivity increases with increasing frequency as expected (any hopping model has this feature) [84]. Above the percolation threshold the electrical response of the percolating network led to a constant AC conductivity [83]. The overall frequency dependency of σ_{AC} is approximated by:

$$\sigma_{AC} = \sigma_{DC} + A\omega^{s} \quad (9)$$

where s is power low exponent [83,85]. The AC electrical conductivity of the TPU/mTRGO reveals the formation of stronger conductive networks which is evidence of the improved dispersion with enhanced interfacial interactions between the mTRGO particles and TPU segments.

Dielectric Permittivity

Fig. 10 (a-c) depicts the variation of the real and imaginary part of complex permittivity (ε^*) versus frequency for neat TPU and the corresponding nanocomposites with different

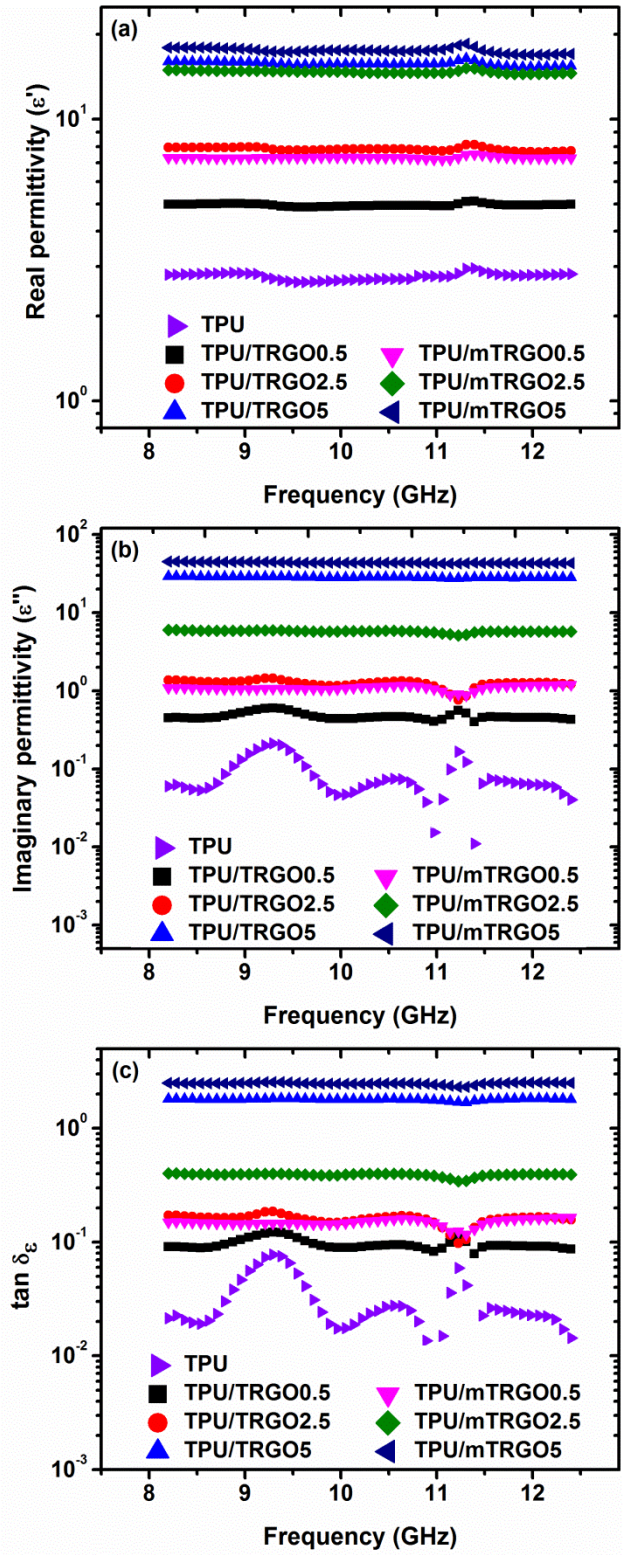

Fig. 10. Effect of functionalization and filler loading on: (a) the real part of permittivity (ε'); (b) the imaginary part of permittivity (ε''); (c) the dielectric loss factor (tan δε).

amounts of TRGO and mTRGO. All composites exhibit an increase in the permittivity with increasing TRGO and mTRGO loading. However, nanocomposites containing mTRGO exhibit a much higher dielectric constant (ε') at comparable loading than TPU/TRGO composites. This is attributed to the increase

in the degree of dipole polarization as a result of functional groups attached to the surface of mTRGO, and also to better dispersion of mTRGO platelets throughout the TPU matrix. In polymer nanocomposites comprising conductive nanofillers, the real part of permittivity represents the number of micro capacitors and polarization centres [47]. Micro-capacitors are generated by the conductive particles or clusters separated by a thin layer of insulating polymer called ligament. Hence, improved dispersion of mTRGO results in a higher number of micro-capacitors which act as interfacial polarization centres. The imaginary permittivity of various prepared composites is presented and compared in Fig. 10(b). Nanocomposites containing mTRGO exhibit higher values for the imaginary permittivity within all studied frequency regions than composites based on TRGO, especially above the percolation threshold of each composite. The significantly enhanced dielectric damping characteristic exhibited by TPU/mTRGO nanocomposites is thought to be due to the higher number of polarization centres, less resistance to current flow, as well as slowing down of various possible polarization processes by the dipoles existing in the structure of the nanocomposites. The latter is suggested to be due to the higher number of dipoles and stronger attractive interactions between the dipoles which results in an increased viscous feature of dipole polarizations which increases the potential of the material to dissipate the energy of electromagnetic wave via the absorption mechanism. These are consistent with the higher viscoelastic damping behaviour measured for the TPU/mTRGO based nanocomposites by DMTA than TPU/TRGO composite counterparts.

EMI shielding properties

Fig. 11 (a-c) illustrates the variation of total shielding effectiveness (SE) and its components, SE_A, SE_R in the X-band frequency range for TPU/TRGO and TPU/mTRGO composites loaded by different levels of graphene particles. For all samples (1 mm thickness), the total EMI SE improves with increasing conductive filler content. As the loading of TRGO sheets increases, the number of interconnected physical networks formed by the TRGO also increases, leading to the higher and intensified interaction with the incoming wave, and hence higher shielding effectiveness by the composite. Moreover, the SE versus frequency curve (Fig. 11(a)) showed a wave-like behaviour. A similar observation has been reported by Basuli *et al.* [86] for a CNT-based nanocomposite. They suggested this was due to the non-uniformity in the size of the discrete conductive networks throughout the polymer. As Fig. 11(a) shows, the nanocomposites presented higher SE especially for the mTRGO concentrations above the percolation threshold (>2.5 vol. %) than that of TPU/TRGO counterparts with the same loadings. It is noteworthy that the nanocomposite based on 5 vol. % of mTRGO exhibited SE of 24.5 dB at 9.5 GHz compared to that of 15 dB for TPU/TRGO composite with 5 vol. % of TRGO. This substantial increase in the SE measured for TPU/mTRGO composites is attributed to the better dispersion of mTRGO particles with their higher interconnectivity and also the larger area of polymer-filler interface to interact with the

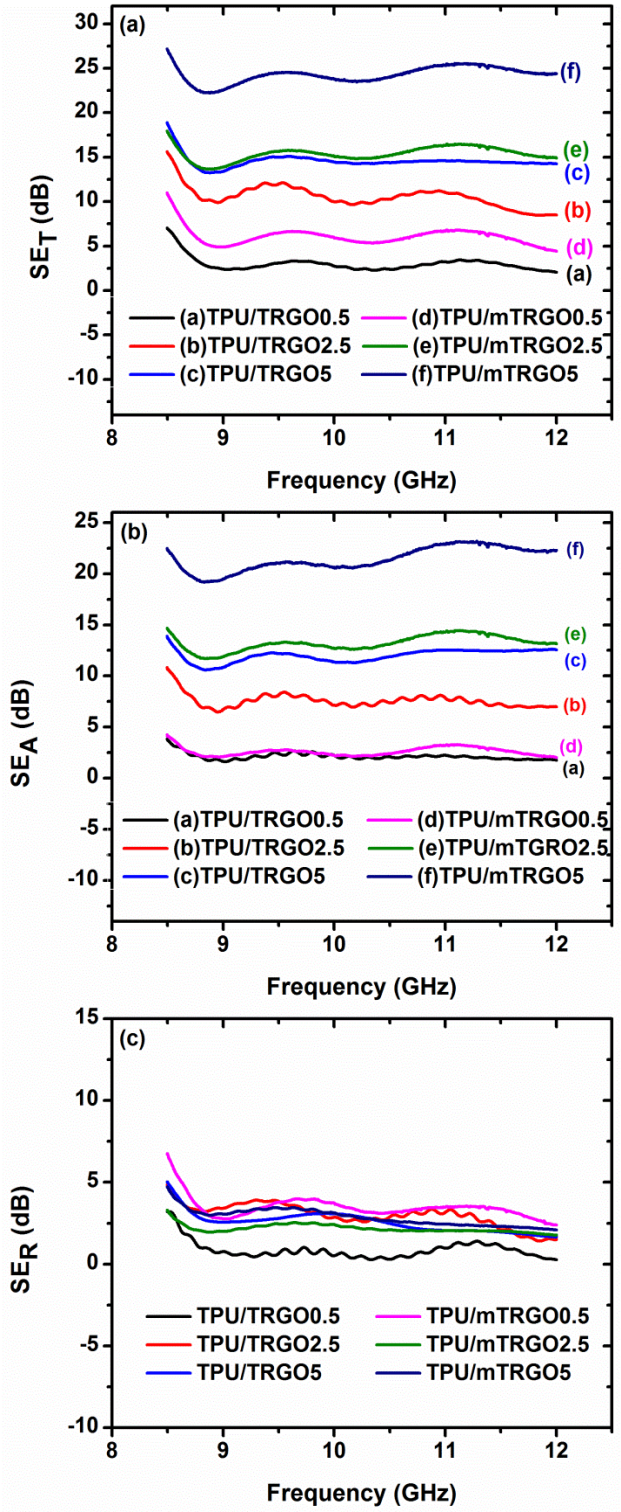

Fig. 11. (a) SE_T, (b) SE_A, and (c) SE_R in the X-band frequency range of TPU/TRGO and TPU/mTRGO nanocomposites.

incident wave [15]. This shows the efficiency of our prepared TPU/mTRGO nanocomposite loaded by 5 vol. % of mTRGO for the attenuation of GHz frequency EM wave to 99.68 % (25 dB) for a sample only 1mm thick.

In order to investigate the relative contribution of reflection and absorption in the total EMI SE of the composites, the SE_A and SE_R were calculated for various

prepared composites directly from S-parameters by using Eq. (4) and (5). Fig. 11 (b, c) compares the SE_A and SE_R of the TPU/TRGO and TPU/mTRGO composites with different filler loading as a function of frequency. As shown in Fig. 11 (c), the shielding by reflection was similar for both groups of composites with no significant increase with filler (TRGO, mTRGO) loading. SE_R reached a maximum of about 4-5 dB. However, the shielding by absorption is dominant and increased significantly with filler content which can be attributed to the increase in interconnectivity of the conductive networks (Fig. 11 (b)). On the other hand, the increasing in SE_A by filler loading is more significant in the case of TPU/mTRGO compared to the TPU/TRGO. While this could be explained by the difference in electrical conductivity (AC, DC) between TPU/mTRGO and TPU/TRGO nanocomposites at comparable filler amounts (Fig. 12), we attest that this conductivity change cannot fully account for the difference. This view is supported by EM shield models that have been widely used to estimate the EMI SE of CPCs based on composite conductivity [7,20,87]. According to this theory, SE_A, and SE_{MR} can be defined with the following equations:

$$SE_A = 20\,log(e^{t/\delta}) = 8.68\,t/\delta \quad (10)$$

$$SE_{MR} = 20\,log\,|1 - e^{-2t/\delta}| \quad (11)$$

where f is frequency of the radiated wave, t is the shield thickness and δ is skin depth ($\delta = \sqrt{\pi f \sigma \mu}^{-1}$). Also for conductive materials ($\sigma \gg \omega\varepsilon$), SE_R can be expressed by Eq. 12 as below:

$$SE_R = 39.5 + 10\,log\,(\frac{\sigma}{2\pi f \mu}) \quad (12)$$

where μ is the magnetic permeability. It should be note that the SE_R calculated using Eq. 12 will yield negative values if $\sigma/f\mu > 7.04 \times 10^{-4}$.

Table 2 compares the theoretical and the experimental EMI SE of nanocomposites containing 5 vol. % of TRGO and mTRGO. For SE_A, the experimental values are 68.5% and 124.8% higher than the theoretical results for TPU/TRGO5 and TPU/mTRGO5, respectively. Such a discrepancy has been reported by others as well [7,20,45,87]. In refs [45] and [20] the authors suggest that these differences might be due to the fact that these models neglect to account for multiple reflections. Furthermore, in [7] the effect of shield thickness on theoretical and experimental SE has been studied and results revealed that a good estimation of SE_A was achieved only for plate thicknesses higher than the skin depth and only at high frequency. However, there was still significant difference between theoretical and experimental SE_A for the

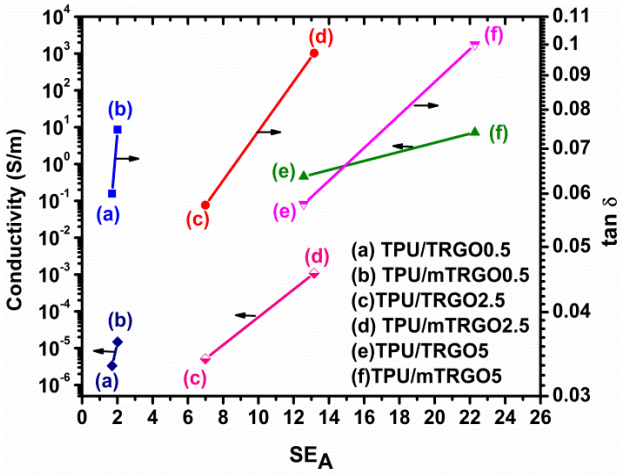

Fig. 12. Electrical conductivity and mechanical loss tangent (at 1 Hz) vs SE_A (at 11 GHz) for TPU/TRGO and TPU/mTRGO containing different filler loading.

shields with higher thickness at lower frequencies. Based on the aforementioned discussions, in addition to the shield thickness, other parameter affected by frequency may also lead to this deviation between theory and experimental results. Since the dissipation of the EM wave energy via absorption is thought to be governed mainly by the extent of conductivity and dielectric polarization [8,88–90], these results lead to the conclusion that in addition to the conductivity, dielectric polarization, which is a frequency dependent phenomenon, plays an important role in the dissipation of EM wave energy via absorption mechanism. As mentioned before, the dielectric polarization and permittivity decreases with frequency. Therefore, the main determining parameter for SE_A in the high frequency region is the shield conductivity. However, orientation polarization and dielectric permittivity impact SE_A more strongly in the low frequency region which can be the reason for the difference between theory and experimental SE_A.

In our system, SE due to multiple reflections should be negligible as SE_A in composites containing 5 vol. % filler is much higher than 10 dB. Therefore, this cannot be the only reason for the deviation between theory and experimental results. Moreover, the theoretical SE_A of TPU/TRGO is very close to the value for TPU/mTRGO nanocomposite which takes into account the conductivity difference. However, there is a significant difference between SE_A of TPU/TRGO5 and TPU/mTRGO5 in the experimental results. This might be attributed to the stronger interfacial interactions between mTRGO and TPU segments as there is a small difference between TPU/TRGO5 and TPU/mTRGO5 electrical conductivity.

Table2. Comparison between theoretical and experimental EMI SE and its components.

Sample	Absorption (dB)				Multiple reflection (dB)	
	9.5 GHz		12 GHz			
	Theory	Exp.	Theory	Exp.	Exp.	Theory
TPU/TRGO5	8.18	12.18	7.42	12.57	Negligible	0
TPU/mTRGO5	10	21.06	9.93	22.28	Negligible	0

Since the orientation dipole polarization is related to the ease of molecular motions, there exists a correlation between dielectric and mechanical losses [52]. In other words, improved dispersion of mTRGO leads to an increase in TPU-mTRGO interfacial area. This amplified interfacial interaction between TPU and the surface functional groups of mTRGO restricts the mobility of TPU segments. Hence, orientation of the dipoles in the direction of the applied field will be more difficult which leads to a higher dissipation of the EM wave energy via absorption. Since these interfacial interactions are difficult to probe by electrical means, the enhancement observed by mechanical means may provide a better indicator for improved shielding by absorption in thinner films. Based on published reports, the dipole rotation or orientational polarization plays the largest role in relaxation loss [91].

Conclusion

In summary, nanocomposites based on TPU and both unmodified and surface functionalized graphene sheets were prepared via a solution mixing process and their EMI shielding response was investigated. The influence of graphene modification on the electrical and dielectric properties were studied for both groups of composites loaded with various levels of filler. Results showed that the TPU/mTRGO composites exhibited a higher electrical conductivity and improved dielectric properties due to the stronger interfacial interaction between the mTRGO and the TPU matrix. The TPU/mTRGO film with 5 vol. % graphene and thickness of 1 mm exhibited commercially relevant EMI SE of ~25 dB in the X-band frequency range. Also, the mechanical damping behaviour and viscoelastic feature of composites was investigated. Functionalization of the graphene surface was found to be effective in increasing the dispersion state and the TPU/graphene interfacial interactions. All composites based on mTRGO presented higher SE compared to TRGO based composites with similar filler loadings. The contribution of SE_A was found to be much higher than SE_R especially in TPU/mTRGO composites. The significant improvement in SE_A of TPU/mTRGO composites is hypothesized to be related to their higher viscoelastic damping behavior in addition to the higher electrical conductivity.

Acknowledgment

The authors would like to thank Charles Dal Castel, Jiaxin Xu, and Dilara Yilman from Chemical Engineering department, University of Waterloo, for their insightful comments and support. The authors also would like to thank financial support from grant NSERC Discovery for part of this project.

References:

[1] P. Saini, M. Arora, G. Gupta, B.K. Gupta, V.N. Singh, V. Choudhary, High permittivity polyaniline-barium titanate nanocomposites with excellent electromagnetic interference shielding response., Nanoscale. 5 (2013) 4330–6. doi:10.1039/c3nr00634d.

[2] S.U.D. Khan, M. Arora, M. a. Wahab, P. Saini, Permittivity and Electromagnetic Interference Shielding Investigations of Activated Charcoal Loaded Acrylic Coating Compositions, J. Polym. 2014 (2014) 1–7. doi:10.1155/2014/193058.

[3] M.H. Al-Saleh, G.A. Gelves, U. Sundararaj, Copper nanowire/polystyrene nanocomposites: Lower percolation threshold and higher EMI shielding, Compos. Part A Appl. Sci. Manuf. 42 (2011) 92–97. doi:10.1016/j.compositesa.2010.10.003.

[4] A. Ameli, P.U. Jung, C.B. Park, Electrical properties and electromagnetic interference shielding effectiveness of polypropylene/carbon fiber composite foams, Carbon N. Y. 60 (2013) 379–391. doi:10.1016/j.carbon.2013.04.050.

[5] C.K. Jang, J.H. Park, J.Y. Jaung, MWNT/PEG grafted nanocomposites and an analysis of their EMI shielding properties, Mater. Res. Bull. 47 (2012) 2767–2771. doi:10.1016/j.materresbull.2012.04.131.

[6] Y. Huang, N. Li, Y. Ma, F. Du, F. Li, X. He, X. Lin, H. Gao, Y. Chen, The influence of single-walled carbon nanotube structure on the electromagnetic interference shielding efficiency of its epoxy composites, Carbon N. Y. 45 (2007) 1614–1621. doi:10.1016/j.carbon.2007.04.016.

[7] M.H. Al-Saleh, U. Sundararaj, X-band EMI shielding mechanisms and shielding effectiveness of high structure carbon black/polypropylene composites, J. Phys. D. Appl. Phys. 46 (2013) 35304. doi:10.1088/0022-3727/46/3/035304.

[8] M. Faisal, S. Khasim, Broadband electromagnetic shielding and dielectric properties of polyaniline-stannous oxide composites, J. Mater. Sci. Mater. Electron. 24 (2013) 2202–2210. doi:10.1007/s10854-013-1080-y.

[9] P. Dinesh, N.M. Renukappa, Siddaramaiah, J. Sundara Rajan, Electrical properties and EMI shielding characteristics of multiwalled carbon nanotubes filled carbon black-high density polyethylene nanocomposites, Compos. Interfaces. 19 (2012) 121–133.

[10] N. Li, Y. Huang, F. Du, X. He, X. Lin, H. Gao, Y. Ma, F. Li, Y. Chen, P.C. Eklund, Electromagnetic Interference (EMI) shielding of single-walled carbon nanotube epoxy composites, Nano Lett. 6 (2006) 1141–1145. doi:10.1021/nl0602589.

[11] J. Liang, Y. Wang, Y. Huang, Y. Ma, Z. Liu, J. Cai, C. Zhang, H. Gao, Y. Chen, Electromagnetic interference shielding of graphene/epoxy composites, Carbon N. Y. 47 (2009) 922–925. doi:10.1016/j.carbon.2008.12.038.

[12] L. Chen, R. Ozisik, L.S. Schadler, The influence of carbon

nanotube aspect ratio on the foam morphology of MWNT/PMMA nanocomposite foams, Polymer (Guildf). 51 (2010) 2368–2375. doi:10.1016/j.polymer.2010.03.042.

[13] P. Dinesh, N.M. Renukappa, Siddaramaiah, J. Sundara Rajan, S. Rajan, Siddaramaiah, J. Sundara Rajan, S. Rajan, Siddaramaiah, J. Sundara Rajan, S. Rajan, Electrical Resistivity and Electromagnetic Interference Shielding Effectiveness of multiwalled carbon nanotubes filled carbon black-high density polyethylene nanocomposites., Compos. Interfaces. 19 (2012) 121–133. doi:10.1080/15685543.2012.699384.

[14] N.C. Das, T.K. Chaki, D. Khastgir, A. Chakraborty, Electromagnetic Interference Shielding Effectiveness of Ethylene Vinyl Acetate Based Conductive Composites, J. Appl. Polym. Sci. 80 (2001) 1601–1608.

[15] S. Maiti, N.K. Shrivastava, S. Suin, B.B. Khatua, Polystyrene / MWCNT / Graphite Nanoplate Nanocomposites : E ffi cient Electromagnetic Interference Shielding Material through Graphite Nanoplate − MWCNT − Graphite Nanoplate Networking, ACS Appl. Mater. Interfaces. 5 (2013) 4712–4724. doi:10.1021/am400658h.

[16] T.K. Gupta, B.P. Singh, S. Teotia, V. Katyal, S.R. Dhakate, R.B. Mathur, Designing of multiwalled carbon nanotubes reinforced polyurethane composites as electromagnetic interference shielding materials, J. Polym. Res. 20 (2013) 32–35. doi:10.1007/s10965-013-0169-6.

[17] S. Das Ramôa, G.M. Barra, R.V. Oliveira, M.G. De Oliveira, M. Cossa, B.G. Soares, Electrical, rheological and electromagnetic interference shielding properties of thermoplastic polyurethane/carbon nanotube composites, Polym. Int. 62 (2013) 1477–1484. doi:10.1002/pi.4446.

[18] A.R. Shafieizadegan-Esfahani, A.A. Katbab, A.R. Pakdaman, P. Dehkhoda, M.H. Shams, A. Ghorbani, Electrically conductive foamed polyurethane/silicone rubber/graphite nanocomposites as radio frequency wave absorbing material: The role of foam structure, Polym. Compos. 33 (2012) 397–403.

[19] M.H. Al-Saleh, W.H. Saadeh, U. Sundararaj, EMI shielding effectiveness of carbon based nanostructured polymeric materials: A comparative study, Carbon N. Y. 60 (2013) 146–156. doi:10.1016/j.carbon.2013.04.008.

[20] C.S. Zhang, Q.Q. Ni, S.Y. Fu, K. Kurashiki, Electromagnetic interference shielding effect of nanocomposites with carbon nanotube and shape memory polymer, Compos. Sci. Technol. 67 (2007) 2973–2980. doi:10.1016/j.compscitech.2007.05.011.

[21] M.H. Al-Saleh, U. Sundararaj, Electromagnetic interference (EMI) shielding effectiveness of PP/PS polymer blends containing high structure carbon black, Macromol. Mater. Eng. 293 (2008) 621–630. doi:10.1002/mame.200800060.

[22] M. Rahaman, T.K. Chaki, D. Khastgir, Development of high performance EMI shielding material from EVA, NBR, and their blends: Effect of carbon black structure, J. Mater. Sci. 46 (2011) 3989–3999. doi:10.1007/s10853-011-5326-x.

[23] A. Das, H.T. Hayvaci, M.K. Tiwari, I.S. Bayer, D. Erricolo, C.M. Megaridis, Superhydrophobic and conductive carbon nanofiber/PTFE composite coatings for EMI shielding, J. Colloid Interface Sci. 353 (2011) 311–315. doi:10.1016/j.jcis.2010.09.017.

[24] S.T. Hsiao, C.C.M. Ma, H.W. Tien, W.H. Liao, Y.S. Wang, S.M. Li, C.Y. Yang, S.C. Lin, R. Bin Yang, Effect of covalent modification of graphene nanosheets on the electrical property and electromagnetic interference shielding performance of a water-borne polyurethane composite, ACS Appl. Mater. Interfaces. 7 (2015) 2817–2826. doi:10.1021/am508069v.

[25] S. Stankovich, D.A. Dikin, R.D. Piner, K.A. Kohlhaas, A. Kleinhammes, Y. Jia, Y. Wu, S.B.T. Nguyen, R.S. Ruoff, Synthesis of graphene-based nanosheets via chemical reduction of exfoliated graphite oxide, Carbon N. Y. 45 (2007) 1558–1565. doi:10.1016/j.carbon.2007.02.034.

[26] Y. Zhu, S. Murali, W. Cai, X. Li, J.W. Suk, J.R. Potts, R.S. Ruoff, Graphene and graphene oxide: Synthesis, properties, and applications, Adv. Mater. 22 (2010) 3906–3924. doi:10.1002/adma.201001068.

[27] T.K. Das, S. Prusty, Graphene-Based Polymer Composites and Their Applications, Polym. Plast. Technol. Eng. 52 (2013) 319–331. doi:10.1080/03602559.2012.751410.

[28] A.A. Al-Ghamdi, F. El-Tantawy, New electromagnetic wave shielding effectiveness at microwave frequency of polyvinyl chloride reinforced graphite/copper nanoparticles, Compos. Part A Appl. Sci. Manuf. 41 (2010) 1693–1701. doi:10.1016/j.compositesa.2010.08.006.

[29] J. Abraham, M. Arif, S. Thomas, A comprehensive study of surface modified graphene based polymer nanocomposites for multifunctional electronic applications, in: Young Res. Vac. Micro/Nano Electron., IEEE, 2016: pp. 1–13.

[30] S.T. Hsiao, C.C.M. Ma, H.W. Tien, W.H. Liao, Y.S. Wang, S.M. Li, Y.C. Huang, Using a non-covalent modification to prepare a high electromagnetic interference shielding performance graphene nanosheet/water-borne polyurethane composite, Carbon N. Y. 60 (2013) 57–66. doi:10.1016/j.carbon.2013.03.056.

[31] S. Chhetri, P. Samanta, N.C. Murmu, S. Kumar, Electromagnetic interference shielding and thermal properties of non- covalently functionalized reduced graphene oxide / epoxy composites, 4 (2017) 61–74.

doi:10.3934/matersci.2017.1.61.

[32] M. Verma, S. Singh, S.K. Dhawan, V. Choudhary, Graphene nanoplatelets / carbon nanotubes / polyurethane composites as ef fi cient shield against electromagnetic polluting radiations, Compos. Part B. 120 (2017) 118–127. doi:10.1016/j.compositesb.2017.03.068.

[33] C.-W. Lou Jia-Horng Lin, Zheng-Ian Lin, Yi-Jun Pan, Chih-Kuang Chen, Chien-Lin Huang, Chen-Hung Huang, Improvement in Mechanical Properties and Electromagnetic Interference Shielding Effectiveness of PVA-Based Composites: Synergistic Effect Between Graphene Nano-Sheets and Multi-Walled Carbon Nanotubes, Macromol. Mater. Eng. 301 (2016) 199–211. doi:10.1002/mame.201500314.

[34] X. Sun, X. Liu, X. Shen, Y. Wu, Z. Wang, J. Kim, Composites : Part A Graphene foam / carbon nanotube / poly (dimethyl siloxane) composites for exceptional microwave shielding, Compos. PART A. (2016). doi:10.1016/j.compositesa.2016.03.009.

[35] J. Chen, J. Wu, H. Ge, D. Zhao, C. Liu, X. Hong, Reduced graphene oxide deposited carbon fiber reinforced polymer composites for electromagnetic interference shielding, Compos. Part A Appl. Sci. Manuf. 82 (2016) 141–150. doi:10.1016/j.compositesa.2015.12.008.

[36] J. Wu, J. Chen, Y. Zhao, W. Liu, W. Zhang, Effect of electrophoretic condition on the electromagnetic interference shielding performance of reduced graphene oxide-carbon fiber/epoxy resin composites, Compos. Part B. (2016). doi:10.1016/j.compositesb.2016.08.042.

[37] M. Verma, S.S. Chauhan, S.K. Dhawan, V. Choudhary, Graphene nanoplatelets/carbon nanotubes/polyurethane composites as efficient shield against electromagnetic polluting radiations, Compos. Part B Eng. 120 (2017) 118–127. doi:10.1016/j.compositesb.2017.03.068.

[38] B. Shen, Y. Li, D. Yi, W. Zhai, X. Wei, W. Zheng, Strong flexible polymer / graphene composite fi lms with 3D saw-tooth folding for enhanced and tunable electromagnetic shielding, Carbon N. Y. 113 (2017) 55–62. doi:10.1016/j.carbon.2016.11.034.

[39] B. Shen, Y. Li, D. Yi, W. Zhai, X. Wei, W. Zheng, Strong flexible polymer/graphene composite films with 3D saw-tooth folding for enhanced and tunable electromagnetic shielding, Carbon N. Y. 113 (2017) 55–62.

[40] X. Luo, D.D.L. Chung, Electromagnetic interference shielding using continuous carbon-fiber carbon-matrix and polymer-matrix composites, Compos. Part B Eng. 30 (1999) 227–231. doi:10.1016/S1359-8368(98)00065-1.

[41] D.D.. Chung, Electromagnetic interference shielding effectiveness of carbon materials, Carbon N. Y. 39 (2001) 279–285. doi:10.1016/S0008-6223(00)00184-6.

[42] M. Mahmoodi, M. Arjmand, U. Sundararaj, S. Park, The electrical conductivity and electromagnetic interference shielding of injection molded multi-walled carbon nanotube/polystyrene composites, Carbon N. Y. 50 (2012) 1455–1464. doi:10.1016/j.carbon.2011.11.004.

[43] A. AF, Z. Abbas, O. SJ, A. Dm, Attenuation Performance of Polymer Composites Incorporating NZF Filler for Electromagnetic Interference Shielding at Microwave Frequencies, J. Mater. Sci. Eng. 5 (2016) 6–11. doi:10.4172/2169-0022.1000289.

[44] S. Pande, B.P. Singh, R.B. Mathur, T.L. Dhami, P. Saini, S.K. Dhawan, Improved electromagnetic interference shielding properties of MWCNT-PMMA composites using layered structures, Nanoscale Res. Lett. 4 (2009) 327–334. doi:10.1007/s11671-008-9246-x.

[45] M.H. Al-Saleh, U. Sundararaj, Electromagnetic interference shielding mechanisms of CNT/polymer composites, Carbon N. Y. 47 (2009) 1738–1746. doi:10.1016/j.carbon.2009.02.030.

[46] A. Gupta, V. Choudhary, Electromagnetic interference shielding behavior of poly(trimethylene terephthalate)/multi-walled carbon nanotube composites, Compos. Sci. Technol. 71 (2011) 1563–1568. doi:10.1016/j.compscitech.2011.06.014.

[47] M. Arjmand, T. Apperley, M. Okoniewski, U. Sundararaj, Comparative study of electromagnetic interference shielding properties of injection molded versus compression molded multi-walled carbon nanotube/polystyrene composites, Carbon N. Y. 50 (2012) 5126–5134. doi:10.1016/j.carbon.2012.06.053.

[48] B. Yuan, L. Yu, L. Sheng, K. An, X. Zhao, Comparison of electromagnetic interference shielding properties between single-wall carbon nanotube and graphene sheet/polyaniline composites., J. Phys. D. Appl. Phys. 45 (2012) 235108/1-235108/6. doi:10.1088/0022-3727/45/23/235108.

[49] Y. Wang, H. Guan, C. Dong, X. Xiao, S. Du, Y. Wang, Reduced graphene oxide (RGO)/Mn3O4 nanocomposites for dielectric loss properties and electromagnetic interference shielding effectiveness at high frequency, Ceram. Int. 42 (2015) 936–942. doi:10.1016/j.ceramint.2015.09.022.

[50] S. George, K.T. Varughese, S. Thomas, Dielectric Properties of Isotactic Polypropylene / Nitrile Rubber Blends : Effects of Blend Ratio , Filler Addition , and Dynamic Vulcanization, J. Appl. Polym. Sci. 73 (1998) 255–270.

[51] H. Valentová, M. Ilčíková, K. Czaniková, Z. Špitalský, M. Šlouf, J. Nedbal, M. Omastová, Dynamic Mechanical and Dielectric Properties of Ethylene Vinyl Acetate/Carbon Nanotube Composites, J. Macromol. Sci. Part B. 53 (2014) 496–512. doi:10.1080/00222348.2013.846814.

[52] B.P. Sahoo, K. Naskar, R.N.P. Choudhary, S. Sabharwal, D.K. Tripathy, Dielectric relaxation behavior of conducting carbon black reinforced ethylene acrylic elastomer vulcanizates, J. Appl. Polym. Sci. 124 (2012) 678–688.

[53] M. Mortezaei, M.H.N. Famili, M. Kokabi, The role of interfacial interactions on the glass-transition and viscoelastic properties of silica/polystyrene nanocomposite, Compos. Sci. Technol. 71 (2011) 1039–1045. doi:10.1016/j.compscitech.2011.02.012.

[54] M. Valentini, F. Piana, J. Pionteck, F.R. Lamastra, F. Nanni, Electromagnetic properties and performance of exfoliated graphite (EG) - Thermoplastic polyurethane (TPU) nanocomposites at microwaves, Compos. Sci. Technol. 114 (2015) 26–33. doi:10.1016/j.compscitech.2015.03.006.

[55] B. Wen, M. Cao, M. Lu, W. Cao, H. Shi, J. Liu, X. Wang, H. Jin, X. Fang, W. Wang, J. Yuan, Reduced graphene oxides: Light-weight and high-efficiency electromagnetic interference shielding at elevated temperatures, Adv. Mater. 26 (2014) 3484–3489. doi:10.1002/adma.201400108.

[56] D.-X. Yan, H. Pang, L. Xu, Y. Bao, P.-G. Ren, J. Lei, Z.-M. Li, Electromagnetic interference shielding of segregated polymer composite with an ultralow loading of *in situ* thermally reduced graphene oxide, Nanotechnology. 25 (2014) 145705. doi:10.1088/0957-4484/25/14/145705.

[57] D.X. Yan, H. Pang, B. Li, R. Vajtai, L. Xu, P.G. Ren, J.H. Wang, Z.M. Li, Structured reduced graphene oxide/polymer composites for ultra-efficient electromagnetic interference shielding, Adv. Funct. Mater. 25 (2015) 559–566. doi:10.1002/adfm.201403809.

[58] D.-X. Yan, P.-G. Ren, H. Pang, Q. Fu, M.-B. Yang, Z.-M. Li, Efficient electromagnetic interference shielding of lightweight graphene/polystyrene composite, J. Mater. Chem. 22 (2012) 18772. doi:10.1039/c2jm32692b.

[59] J. Ling, W. Zhai, W. Feng, B. Shen, J. Zhang, W.G. Zheng, Facile preparation of lightweight microcellular polyetherimide/graphene composite foams for electromagnetic interference shielding, ACS Appl. Mater. Interfaces. 5 (2013) 2677–2684. doi:10.1021/am303289m.

[60] H. Bin Zhang, W.G. Zheng, Q. Yan, Z.G. Jiang, Z.Z. Yu, The effect of surface chemistry of graphene on rheological and electrical properties of polymethylmethacrylate composites, Carbon N. Y. 50 (2012) 5117–5125. doi:10.1016/j.carbon.2012.06.052.

[61] A.P. Singh, P. Garg, F. Alam, K. Singh, R.B. Mathur, R.P. Tandon, A. Chandra, S.K. Dhawan, Phenolic resin-based composite sheets filled with mixtures of reduced graphene oxide, γ-Fe 2O 3 and carbon fibers for excellent electromagnetic interference shielding in the X-band, Carbon N. Y. 50 (2012) 3868–3875. doi:10.1016/j.carbon.2012.04.030.

[62] C. Li, G. Yang, H. Deng, K. Wang, Q. Zhang, F. Chen, Q. Fu, The preparation and properties of polystyrene/functionalized graphene nanocomposite foams using supercritical carbon dioxide, Polym. Int. 62 (2013) 1077–1084. doi:10.1002/pi.4394.

[63] S. Maiti, N.K. Shrivastava, S. Suin, B.B. Khatua, Polystyrene/MWCNT/graphite nanoplate nanocomposites: efficient electromagnetic interference shielding material through graphite nanoplate–MWCNT–graphite nanoplate networking, ACS Appl. Mater. Interfaces. 5 (2013) 4712–4724. doi:10.1021/am400658h.

[64] H. Zhang, Q. Yan, W. Zheng, Z. He, Z. Yu, Tough Graphene - Polymer Microcellular Foams for Electromagnetic Interference Shielding, ACS Appl. Mater. Interfaces. 3 (2011) 918–924. doi:10.1021/am200021v.

[65] A. Bhattacharyya, M. Joshi, Functional properties of microwave-absorbent nanocomposite coatings based on thermoplastic polyurethane-based and hybrid carbon-based nanofillers, Polym. Adv. Technol. 23 (2012) 975–983. doi:10.1002/pat.2000.

[66] E. Jayamani, S. Hamdan, M.R. Rahman, M.K. Bin Bakri, Comparative study of dielectric properties of hybrid natural fiber composites, Procedia Eng. 97 (2014) 536–544. doi:10.1016/j.proeng.2014.12.280.

[67] H.C. Schniepp, J.L. Li, M.J. McAllister, H. Sai, M. Herrera-Alonson, D.H. Adamson, R.K. Prud'homme, R. Car, D.A. Seville, I.A. Aksay, Functionalized single graphene sheets derived from splitting graphite oxide, J. Phys. Chem. B. 110 (2006) 8535–8539. doi:10.1021/jp060936f.

[68] D.C. Marcano, D. V. Kosynkin, J.M. Berlin, A. Sinitskii, Z. Sun, A. Slesarev, L.B. Alemany, W. Lu, J.M. Tour, Improved synthesis of graphene oxide, ACS Nano. 4 (2010) 4806–4814. doi:10.1021/nn1006368.

[69] T. Huang, Y. Xin, T. Li, S. Nutt, C. Su, H. Chen, P. Liu, Z. Lai, Modified graphene/polyimide nanocomposites: reinforcing and tribological effects, ACS Appl. Mater. Interfaces. 5 (2013) 4878–4891.

[70] M. Fang, K. Wang, H. Lu, Y. Yang, S. Nutt, Single-layer graphene nanosheets with controlled grafting of polymer chains, J. Mater. Chem. 20 (2010) 1982–1992. doi:10.1039/b919078c.

[71] H. Kim, Y. Miura, C.W. MacOsko, Graphene/polyurethane nanocomposites for improved gas barrier and electrical conductivity, Chem. Mater. 22 (2010) 3441–3450. doi:10.1021/cm100477v.

[72] H. Zhang, W. Zheng, Q. Yan, Y. Yang, J. Wang, Z. Lu, G. Ji, Z. Yu, Electrically conductive polyethylene terephthalate / graphene nanocomposites prepared by melt compounding, Polymer (Guildf). 51 (2010) 1191–1196. doi:10.1016/j.polymer.2010.01.027.

[73] M.J. Mcallister, J. Li, D.H. Adamson, H.C. Schniepp, A. a Abdala, J. Liu, O.M. Herrera-alonso, D.L. Milius, R. Car, R.K. Prud, I. a Aksay, Single Sheet Functionalized Graphene by Oxidation and Thermal Expansion of Graphite, Am. Chem. Soc. 19 (2007) 4396–4404. doi:10.1021/cm0630800.

[74] J. Liang, Y. Huang, L. Zhang, Y. Wang, Y. Ma, T. Cuo, Y. Chen, Molecular-level dispersion of graphene into poly(vinyl alcohol) and effective reinforcement of their nanocomposites, Adv. Funct. Mater. 19 (2009) 2297–2302. doi:10.1002/adfm.200801776.

[75] B. Yu, X. Wang, W. Xing, H. Yang, L. Song, Y. Hu, UV-Curable Functionalized Graphene Oxide/Polyurethane Acrylate Nanocomposite Coatings with Enhanced Thermal Stability and Mechanical Properties, Ind. Eng. Chem. Res. 51 (2012) 14629–14636. doi:10.1021/ie3013852.

[76] J. Bian, H.L. Lin, F.X. He, X.W. Wei, I.T. Chang, E. Sancaktar, Fabrication of microwave exfoliated graphite oxide reinforced thermoplastic polyurethane nanocomposites: Effects of filler on morphology, mechanical, thermal and conductive properties, Compos. Part A Appl. Sci. Manuf. 47 (2013) 72–82. doi:10.1016/j.compositesa.2012.12.009.

[77] E. Aram, M. Ehsani, H.A. Khonakdar, S.H. Jafari, N.R. Nouri, Functionalization of graphene nanosheets and its dispersion in PMMA/PEO blend: Thermal, electrical, morphological and rheological analyses, Fibers Polym. 17 (2016) 174–180. doi:10.1007/s12221-016-5827-y.

[78] J.-F. Dai, G.-J. Wang, L. Ma, C. Wu, Surface properties of graphene: Relationship to graphene-polymer composites, Rev. Adv. Mater. Sci. 40 (2015) 60–71.

[79] Q. Liu, X. Zhou, X. Fan, C. Zhu, X. Yao, Z. Liu, Mechanical and thermal properties of epoxy resin nanocomposites reinforced with graphene oxide, Polym. Plast. Technol. Eng. 51 (2012) 251–256.

[80] L. Tang, Y. Wan, D. Yan, Y. Pei, L. Zhao, Y. Li, The effect of graphene dispersion on the mechanical properties of graphene / epoxy composites, Carbon N. Y. 60 (2013) 16–27. doi:10.1016/j.carbon.2013.03.050.

[81] P.C. Ma, J.K. Kim, B.Z. Tang, Effects of silane functionalization on the properties of carbon nanotube/epoxy nanocomposites, Compos. Sci. Technol. 67 (2007) 2965–2972. doi:10.1016/j.compscitech.2007.05.006.

[82] J.K. Mishra, K.J. Hwang, C.S. Ha, Preparation, mechanical and rheological properties of a thermoplastic polyolefin (TPO)/organoclay nanocomposite with reference to the effect of maleic anhydride modified polypropylene as a compatibilizer, Polymer (Guildf). 46 (2005) 1995–2002. doi:10.1016/j.polymer.2004.12.044.

[83] S. Barrau, P. Demont, A. Peigney, C. Laurent, C. Lacabanne, Dc and ac conductivity of carbon nanotubes-polyepoxy composites, Macromolecules. 36 (2003) 5187–5194. doi:10.1021/ma021263b.

[84] H.M. Zaki, AC conductivity and frequency dependence of the dielectric properties for copper doped magnetite, Phys. B Condens. Matter. 363 (2005) 232–244. doi:10.1016/j.physb.2005.03.026.

[85] K.-M. Jäger, D.H. McQueen, I.A. Tchmutin, N.G. Ryvkina, M. Klüppel, Electron transport and ac electrical properties of carbon black polymer composites, J. Phys. D. Appl. Phys. 34 (2001) 2699. doi:10.1088/0022-3727/34/17/319.

[86] U. Basuli, S. Chattopadhyay, C. Nah, T.K. Chaki, Electrical properties and electromagnetic interference shielding effectiveness of multiwalled carbon nanotubes-reinforced EMA nanocomposites, Polym. Compos. 33 (2012) 897–903.

[87] K. Nasouri, A.M. Shoushtari, M.R.M. Mojtahedi, Theoretical and experimental studies on EMI shielding mechanisms of multi-walled carbon nanotubes reinforced high performance composite nanofibers, J. Polym. Res. 23 (2016) 3–10. doi:10.1007/s10965-016-0943-3.

[88] L. Shunhua, G. Hongtao, Investigation of electrical conductivity and electromagnetic shielding effectiveness of polyaniline composite, Sci. Technol. Adv. Mater. 6 (2005) 513–518. doi:10.1016/j.stam.2005.01.002.

[89] D.A. Makeiff, T. Huber, Microwave absorption by polyaniline-carbon nanotube composites, Synth. Met. 156 (2006) 497–505. doi:10.1016/j.synthmet.2005.05.019.

[90] N. Gandhi, K. Singh, A. Ohlan, D.P. Singh, S.K. Dhawan, Thermal, dielectric and microwave absorption properties of polyaniline-CoFe2O4 nanocomposites, Compos. Sci. Technol. 71 (2011) 1754–1760. doi:10.1016/j.compscitech.2011.08.010.

[91] N. Noda, Y. Lee, A.J. Bur, V.M. Prabhu, C.R. Snyder, S.C. Roth, M. Mcbrearty, Dielectric properties of nylon 6 / clay nanocomposites from on-line process monitoring and off-line measurements, Polymer (Guildf). 46 (2005) 7201–7217. doi:10.1016/j.polymer.2005.06.046.

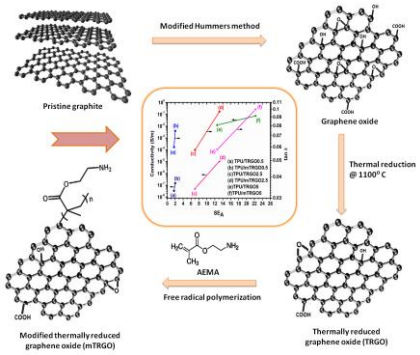

Highlights

- Covalent modification of thermally reduced graphene oxide (TRGO) was performed by grafting 2-aminoethyl methacrylate on the graphene surface.
- Polymer nanocomposites of TPU/TRGO and TPU/mTRGO were prepared by solution mixing.
- Covalent modification of graphene enhances interfacial interactions and mechanical damping.
- The higher electromagnetic interference shielding effectiveness (EMI SE) was 25 dB (99.7% attenuation) achieved in the TPU/mTRGO5 nanocomposite.
- Results demonstrated that dielectric damping and SE via absorption mechanism can be influenced by viscoelastic energy dissipation.